NANO LETTERS
Letter
pubs.acs.org/NanoLett

Low-Frequency Electronic Noise in Quasi-1D $TaSe_3$ van der Waals Nanowires

Guanxiong Liu,[†] Sergey Rumyantsev,[‡,§] Matthew A. Bloodgood,[∥] Tina T. Salguero,[∥] Michael Shur,[‡] and Alexander A. Balandin*,[†]

[†]Nano-Device Laboratory (NDL) and Phonon Optimized Engineered Materials (POEM) Center, Department of Electrical and Computer Engineering, University of California, Riverside, Riverside, California 92521, United States

[‡]Department of Electrical, Computer, and Systems Engineering, Center for Integrated Electronics, Rensselaer Polytechnic Institute, Troy, New York 12180, United States

[§]Ioffe Institute, St. Petersburg 194021, Russia

[∥]Department of Chemistry, University of Georgia, Athens, Georgia 30602, United States

ABSTRACT: We report results of investigation of the low-frequency electronic excess noise in quasi-1D nanowires of $TaSe_3$ capped with quasi-2D *h*-BN layers. Semimetallic $TaSe_3$ is a quasi-1D van der Waals material with exceptionally high breakdown current density. It was found that $TaSe_3$ nanowires have lower levels of the normalized noise spectral density, S_I/I^2, compared to carbon nanotubes and graphene (I is the current). The temperature-dependent measurements revealed that the low-frequency electronic $1/f$ noise becomes the $1/f^2$ type as temperature increases to ∼400 K, suggesting the onset of electromigration (f is the frequency). Using the Dutta−Horn random fluctuation model of the electronic noise in metals, we determined that the noise activation energy for quasi-1D $TaSe_3$ nanowires is approximately $E_P \approx 1.0$ eV. In the framework of the empirical noise model for metallic interconnects, the extracted activation energy, related to electromigration is $E_A = 0.88$ eV, consistent with that for Cu and Al interconnects. Our results shed light on the physical mechanism of low-frequency $1/f$ noise in quasi-1D van der Waals semimetals and suggest that such material systems have potential for ultimately downscaled local interconnect applications.

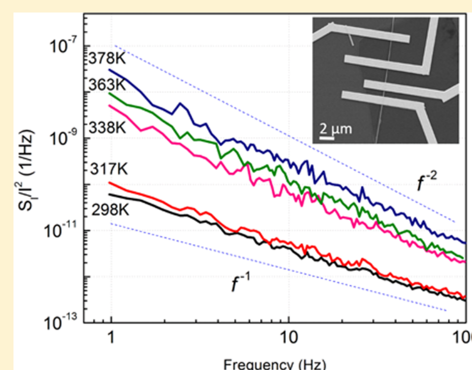

KEYWORDS: *Quasi-1D, van der Waals materials, low-frequency noise, interconnects, reliability*

The investigations of two-dimensional layers and heterostructures have revealed new physics and demonstrated promising applications.[1−14] Starting with graphene,[3−5] and spreading to a wide range of layered van der Waals materials,[6−10] successful isolation of individual atomic layers from their respective bulk crystals by mechanical exfoliation led to the fast growing research activities in the 2D materials field. In contrast to the layered van der Waals materials that yield 2D crystals, materials such as $TaSe_3$ and TiS_3[15−17] yield the quasi-one-dimensional (1D) van der Waals crystal structures. These materials belong to the group of transition metal trichalcogenides MX_3 (where M = Mo, W, and other transition metals; X = S, Se, and Te). In the monoclinic crystal structure of $TaSe_3$, the trigonal prismatic $TaSe_3$ units form continuous chains extending along the *b*-axis and leading to fiber- and needle-like crystals with anisotropic semimetallic or metallic properties. The quasi-1D atomic threads are weakly bound in bundles by van der Waals forces. As a consequence, the mechanical exfoliation of the MX_3 crystals results not in 2D layers but rather in quasi-1D van der Waals nanowires. We have recently demonstrated quasi-1D $TaSe_3$ nanowires with the record high current density exceeding $J_B \sim 30$ MA/cm^2, which is an order of magnitude larger than that for Cu interconnects.[18]

In this Letter, we report on the excess low-frequency electronic noise in quasi-1D nanowires of $TaSe_3$ capped with quasi-2D *h*-BN layers. The *h*-BN capping was used as a surface passivation protecting from environmental exposure. The measurements were performed in the temperature range from 300 to 430 K in order to elucidate the physical mechanism of the low-frequency noise and determine the noise activation energies. The low-frequency noise is a ubiquitous phenomenon present in all kinds of electronic devices including field-effect transistors, diodes, and interconnects.[19−21] The frequency dependence and temperature characteristics of the spectral density of the low-frequency noise have been used as reliability metrics for interconnects in Si complementary metal−oxide−semiconductor (CMOS) technology. The low-frequency noise data at elevated temperatures are directly correlated with the electromigration failure mechanisms in interconnects.[22−24] It

Received: October 17, 2016
Revised: November 22, 2016
Published: November 28, 2016

ACS Publications © XXXX American Chemical Society

DOI: 10.1021/acs.nanolett.6b04334
Nano Lett. XXXX, XXX, XXX−XXX

has been suggested that the low-frequency noise at high temperatures originates from the vacancy migration along the grain boundaries.[22,25] Hence, the noise can reveal information on the electromigration failure of interconnects and metal thin films. The noise activation energies extracted from the two commonly accepted physical models, the Dutta–Horn model[21,24] and the empirical noise model in metals,[22,26,27] have shown an excellent agreement with the activation energies obtained from the industry standard electromigration mean-time-to-failure (MTF) tests. These considerations explain additional practical motivations for investigation of the low-frequency noise in quasi-1D nanowires of $TaSe_3$, which exhibit promise as ultimately downscaled local interconnects owing to their single-crystal atomic thread structure and exceptionally high breakdown current density.[18]

The bulk $TaSe_3$ crystals were synthesized by the chemical vapor transport (CVT) method and then solvent and mechanically exfoliated (see Methods section). The high quality of both bulk and exfoliated quasi-1D $TaSe_3$ samples has been confirmed using a variety of experimental techniques including high-resolution transmission electron microscopy, Raman spectroscopy, energy dispersive spectroscopy, powder X-ray diffraction, and electron probe microanalysis, as reported previously.[18] The devices for the low-frequency noise measurement were fabricated by the mechanical exfoliation of quasi-1D $TaSe_3$ nanowires on Si/SiO_2 substrates. We used the dry transferred *h*-BN flakes to protect the quasi-1D $TaSe_3$ nanowire channels from oxidation and chemical exposure during the fabrication processes. The devices were fabricated by standard e-beam lithography and e-beam metal evaporation.[28] In order to make an electrical connection to the quasi-1D channels, we opened the contact area by dry etching the *h*-BN thin film and the underlying $TaSe_3$ nanowire while leaving the edge of quasi-1D channels in contact with the metal. Figure 1b shows a scanning electron microscopy (SEM) image of $TaSe_3$ crystals prepared by the CVT method. A high-resolution scanning transmission electron microscopy (STEM) inspection (Figure 1a) confirmed a single crystal nature of the material. Figure 1c is a SEM image of representative devices used for the current voltage ($I-V$) and electronic noise measurements.

Figure 2 presents typical $I-V$ characteristics of the devices with different channel lengths. The perfectly linear $I-V$s at low electric fields indicate a high-quality electrical contact between the metal electrode and the quasi-1D $TaSe_3$ nanowire. The *h*-BN capping was essential for achieving good Ohmic contacts between the metal electrodes and the $TaSe_3$ channel. The primary function of the *h*-BN capping layer was to prevent the oxidation during the fabrication, particularly before the final processing step of electrode metal deposition. Etching the *h*-BN capping before the last step of metal deposition ensured clean channel material for contacting with the electrode metal. Additional details of the *h*-BN capping and etching procedures have been reported by us elsewhere.[11,18] The value of the contact resistance for a typical *h*-BN-capped quasi-1D $TaSe_3$ device, determined from the transmission line measurements, was ~22 Ω μm.[18] The inset to Figure 2 shows an optical image of a representative device used in this study. The light blue stripe between metal electrodes is the quasi-1D $TaSe_3$ nanowire while the green region is the *h*-BN capping layer. The brown background is the Si/SiO_2 substrate.

The low-frequency noise measurements were performed at both UCR and RPI using in-house built experimental setups. The equipment included a "quiet" battery, a potentiometer

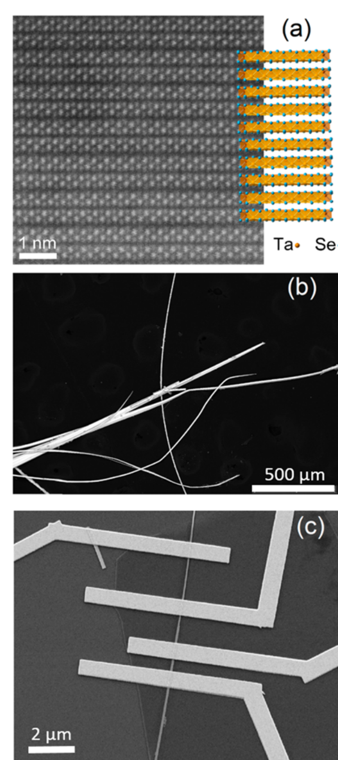

Figure 1. (a) High-resolution scanning transmission electron microscopy image of exfoliated $TaSe_3$ showing pristine metal trichalcogenide chains that extend along the *b*-axis. (b) Scanning electron microscopy image of $TaSe_3$ crystals prepared by the CVT method. (c) SEM image of representative quasi-1D $TaSe_3$ devices.

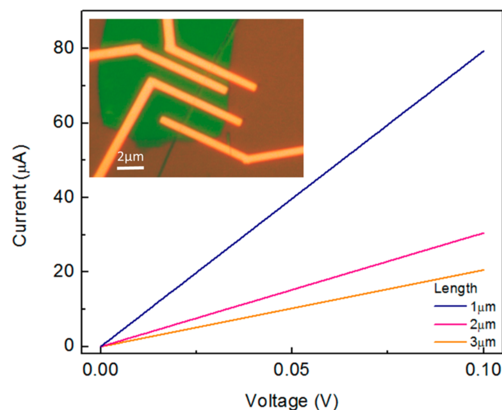

Figure 2. Current–voltage characteristics of $TaSe_3$ devices with different channel lengths. The linear characteristics at low voltage indicates good Ohmic contact of $TaSe_3$ channel with the metal electrodes. The optical microscopy image of the devices is shown in the inset. The quasi-1D $TaSe_3$ channel (light blue) is covered with *h*-BN capping layer (green area), which acts as protection layer against oxidation and environmental exposure. The metal electrodes, in contact with $TaSe_3$ channel at the edges, are fabricated by etching through *h*-BN capping layer.

biasing circuit, a low noise amplifier, and a spectrum analyzer. The details of our noise measurement procedures have been reported elsewhere.[28,29] Figure 3a shows a typical normalized noise spectral density $S_I/I^2 \propto 1/f^\gamma$ with $\gamma = 1.16$ (here I is the channel source–drain current) in the$TaSe_3$ nanowires with 20 nm × 110 nm cross section. The measurements were performed at room temperature (RT). The noise spectral

DOI: 10.1021/acs.nanolett.6b04334
Nano Lett. XXXX, XXX, XXX–XXX

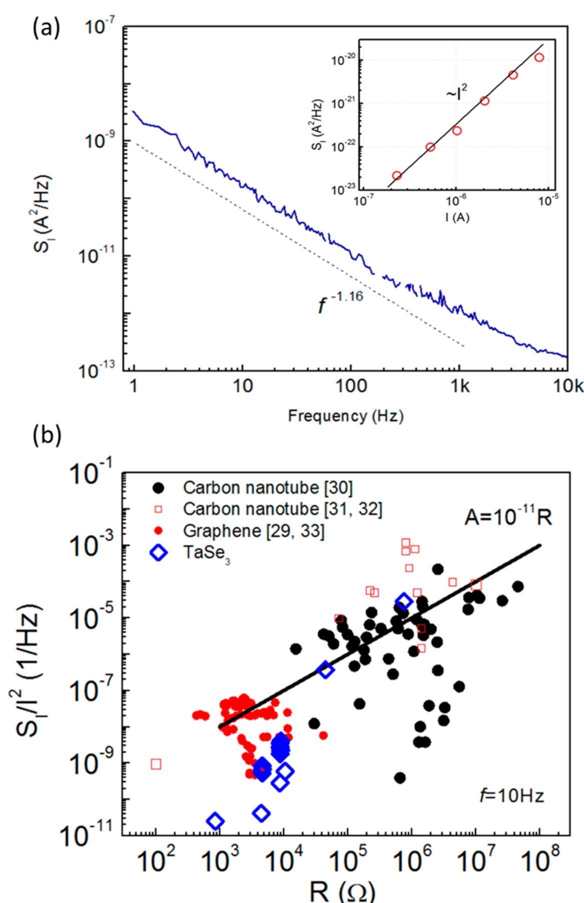

Figure 3. (a) Typical noise spectrum of $TaSe_3$ devices at room temperature. The noise spectrum S_I is flowing $1/f^{\gamma}$ dependence with $\gamma = 1.1-1.2$. The inset shows the noise level at $f = 10$ Hz as the function of the channel (source−drain) current spanning from 0.2 to 10 μA. The quadratic dependence of the noise spectrum density S_I on the channel current I indicates that the $1/f$ noise measured at this current level originates from the $TaSe_3$ device itself rather than the current-induced effects. (b) Normalized noise spectrum density as a function of the resistance for different low-dimensional material systems: quasi-1D $TaSe_3$ nanowires, graphene, and carbon nanotubes. For comparison, the empirical relation $A = 10^{-11}R$ for the low-frequency noise versus resistance R derived from the carbon nanotube studies[29,31−33] is also shown. The noise in quasi-1D $TaSe_3$ nanowires is about 1 order of magnitude lower than that in graphene.

density was determined for currents in the 1−5 μA range, which is sufficiently small to exclude the current induced effects such as electromigration. The latter is confirmed by the perfectly quadratic dependence of the noise spectral density on the source−drain current, i.e., $S_I \propto I^2$. The noise spectral density as a function of the source−drain current is shown in the inset to Figure 3a. The noise spectrum was collected for the two-terminal device. Since the contact resistance is very small compared to that of the channel, the contact noise is considered negligible.[18]

The first interesting observation from the experimental data is that the noise level in $TaSe_3$ nanowires is rather low in comparison with other low-dimensional materials, such as carbon nanotubes and graphene, which also have been proposed for interconnect applications. The normalized noise spectral density, S_I/I^2, for $TaSe_3$ nanowires as a function of the resistance is shown in Figure 3b. The data points for carbon nanotubes[30−32] and graphene[29,33] are presented for comparison. The guide line is the noise amplitude, $A = S_I/I^2 \times f$, which was empirically obtained for the carbon nanotubes.[30] The devices with a lower resistance tend to have a lower level of the low-frequency noise. As one can see, the noise level, expressed as S_I/I^2, in quasi-1D $TaSe_3$ nanowires is about 1 order of magnitude lower than that in graphene.[29,33] It is comparable to the lowest reported values for the carbon nanotubes.[30−32] Most of the tested carbon nanotube devices had a larger resistance and, as a result, a larger noise spectral density. The higher levels of $1/f$ noise typically are associated with a higher density of structural defects as well as mechanical and electromigration damage.[22,25] One should keep in mind that the metal contact with carbon nanotubes or graphene is usually less Ohmic than that with $TaSe_3$. It is likely that carbon nanotubes or graphene devices have substantially higher contact noise contribution than $TaSe_3$ devices.

The resistivity of quasi-1D $TaSe_3$ nanowires increases with temperature, similar to other metallic materials. The inset to Figure 4 shows the resistivity change in the temperature range

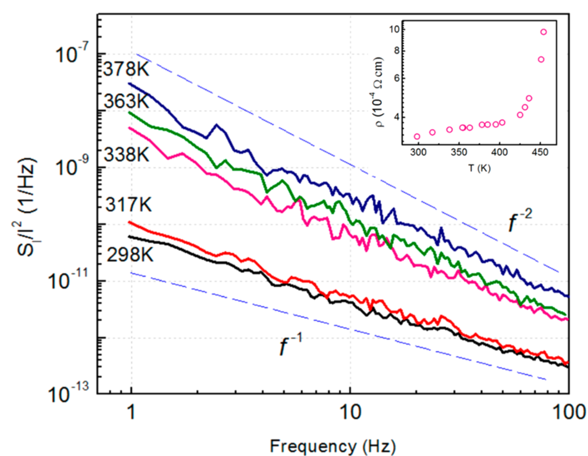

Figure 4. Normalized noise spectra density S_I/I^2 measured for the quasi-1D $TaSe_3$ nanowire at different temperatures. The $1/f$ noise at room temperature becomes more of $1/f^2$ type at elevated temperatures. The increased frequency power factor γ suggests the onset of the electromigration processes. The inset shows the temperature-dependent resistance of the quasi-1D $TaSe_3$ nanowire measured in the range from 300 to 450 K. The graduate increase of the resistance with temperature for $T < 410$ K is typical for metal. The sharply rising resistance for $T > 410$ K indicates the occurrence of electromigration.

from 298 to 450 K. The gradual and relatively slow resistance increase below 420 K is due to increasing electron−phonon scattering, which is common in metals. The sharp increase in resistance at the temperatures above 420 K is likely related to the onset of electromigration as commonly observed in the conventional interconnect reliability tests.[24,34] The $TaSe_3$ nanowire noise spectral density and the frequency exponent γ rapidly grow with temperature (see Figure 4). The noise level at 378 K increases by a factor of ×10 at 100 Hz and a factor of ×300 at 1 Hz compared to that at 298 K. The noise magnitude grows faster at the lower frequencies, changing the type of frequency dependence of the normalized noise spectral density, S_I/I^2, at high temperature.

To better understand the evolution of the low-frequency noise with temperature, we plotted the frequency exponent γ and the normalized noise spectral density, S_I/I^2, as the functions of temperature in the range from 298 to 431 K. The experimental data points in Figure 5a,b are shown for two

DOI: 10.1021/acs.nanolett.6b04334
Nano Lett. XXXX, XXX, XXX−XXX

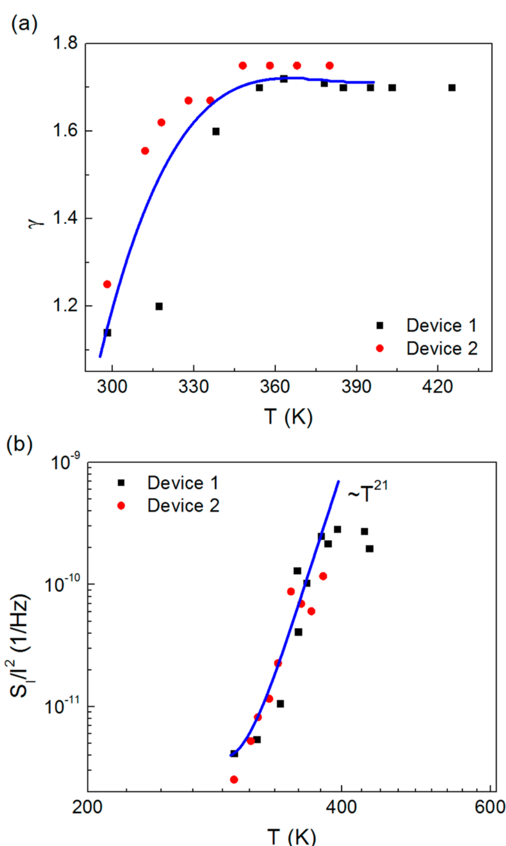

Figure 5. (a) Extracted frequency power factor γ as the function of temperature. The frequency power factor γ increases from 1.16−1.24 at 298 K to 1.72−1.75 at 350 K and remains approximately constant at 1.71−1.75 above 350 K. The blue curve is the fitting of the experimental data. (b) Evolution of the normalized noise spectra density S_I/I^2 with temperature T at frequency 10 Hz. The blue curve is calculated from the Dutta−Horn model. The activation energy estimated from the Dutta−Horn model is E_P = 1.01 eV.

representative devices with different channel cross-section areas at the frequency f = 10 Hz. The frequency exponent γ increases from 1.16−1.24 at 298 K to 1.72−1.75 at 350 K. At temperatures above 350 K, γ remains nearly constant at 1.71−1.75 (see Figure 5a). In Figure 5b, one can see that the noise level increases by 2 orders of magnitude as temperature changes from 298 to 400 K. The data in Figure 5b suggest that the noise spectral density attains its maximum value at T = 400 K and then reveal a saturation and a slowly decreasing trend. This behavior is analogous to that in thin films of Ag and Cu.[35,36] In the region of the fast growth, $S_I/I^2 \sim T^s$ with s = 21 for the shown data set for two representative devices (see Figure 5b).

We now turn to the analysis of the experimental data using two different physical models. The Dutta−Horn model describes the temperature-dependent low-frequency noise by the thermally activated random fluctuations.[35] Within this model, the noise spectral density, $S(f,T)$, can be approximated as

$$S(f,\,T) \propto \frac{kT}{2\pi f} D(E) \tag{1}$$

where $D(E)$ is the distribution density function of the activation energies E and $S(f,T)$ is the spectral noise density. In the limit of the constant $D(E)$ the model leads to the exact $1/f$ noise (γ = 1). The experimentally observed deviations from γ = 1 and temperature dependence of the noise indicate that $D(E)$ is not a constant. One should note here that the maximum in the $S(f,T)$ dependence on temperature does not always coincide with the maximum of $D(E)$ function. The temperature dependence of the frequency exponent γ is expressed as[35]

$$\gamma(T) = 1 - \frac{1}{\ln(2\pi f\tau_0)}\left(\frac{\partial \ln S(f,\,T)}{\partial \ln T} - 1\right) \tag{2}$$

Here τ_0 is characteristic time constant referred to as the attempt escape time. In the original Dutta−Horn model, the time constant τ_0 was assumed to be $\sim 10^{-14}$ s, which is the typical attempt escape time for random processes in solids. The exact value of τ_0 does not strongly affect the low-frequency noise analysis. The blue curve in Figure 5a is a polynomial fit to the experimental data used in the further analysis.

In Figure 5b, the blue line is calculated using eq 2 with the approximated dependence of the frequency exponent γ on temperature shown in Figure 5a. One can see that the Dutta−Horn model describes accurately the temperature dependence of the noise for T < 380 K. The saturation or even the decrease of noise at higher temperatures cannot be explained by this model. The latter is likely related to the onset of another low-frequency noise mechanism. For this reason, applying of the Dutta−Horn model for temperatures above ~400 K has to be done with caution. The activation energy E_P at which the distribution function $D(E)$ attains its peak is related to temperature as

$$E_P = -kT\,\ln(2\pi f\tau_0) \tag{3}$$

The activation energy distribution calculated from the noise data in metals usually has a peak at $E_P \approx 1$ eV.[35] Using the data for a representative device heated all the way to 430 K, we determined that the energy distribution reaches its maximum at $E_P \approx 1.0$ eV for $TaSe_3$ nanowires as well (data set for "Device 1" in Figure 5b). In a more conservative approach, increasing the temperature only to ~390 K, within the application domain of the Dutta−Horn model (data set for "Device 2" in Figure 5b), we determine the low bound of the position of the maximum of the activation energy distribution function $D(E)$. This value is somewhat smaller but still close to ~1 eV.

The noise spectral density $S_I/I^2 \sim 1/f^\gamma$ with $\gamma \approx 2$ in metals is often attributed to the effects of electromigration. Although the detailed mechanism of the resistance fluctuations in metal films has not been established yet, many experiment indicate that the low-frequency noise, electromigration, and degradation in metals are related. The $1/f^\gamma$ noise spectral density with $\gamma \geq 2$, which appears at high temperatures, has been widely used to extract the electromigration activation energy for interconnects. The frequency exponents as high as $\gamma > 4$ have been reported.[37] Attributed to the vacancy migration, $1/f^\gamma$ noise has been proposed as a useful diagnostic tool.[25] It was found that the low-frequency noise at high temperature follows the empirical equation[22]

$$S(f) = \frac{Aj^3}{Tf^\gamma}\exp\!\left(-\frac{E_A}{kT}\right) \tag{4}$$

where A is a constant, j is the biasing current density, and E_A is the activation energy related to electromigration. By measuring the temperature dependence of the noise spectrum, one can extract the activation energy, E_A, from the Arrhenius plot of $T \times S(f)$. A large number of experiments have demonstrated that

DOI: 10.1021/acs.nanolett.6b04334
Nano Lett. XXXX, XXX, XXX−XXX

the E_A values extracted from the low-frequency noise measurements are very close to those obtained from the conventional mean-time-to-failure test for interconnects fabricated with different technology and various metals, including Al, Al alloys, and Cu.[21,23,24,38] The noise measurements have specific advantages over the conventional reliability tests, which require time-dependent resistance measurements of interconnects under high temperature and high current stress for long periods of time (typically from 10 to 100 h for each set). The noise measurements can be conducted in much shorter period of time. They are also be nondestructive. It was found that the noise level often increases rapidly before the sharp resistance increase, which was defined as the interconnect failure.[24]

Figure 6 shows the Arrhenius plot of $T \times S_I/I^2$ vs $1000/T$ for f = 10 Hz. The extracted E_A of 0.88 eV is within the range reported for other metal films. Table 1 summarizes the electromigration activation energy estimated using the $1/f$ noise measurements for different interconnects. The values of the electromigration activation energy for the Cu and Al interconnects determined from the $1/f$ noise measurements are 0.76−1.10 and 0.67−1.14 eV, respectively.[21,22,24,37,39] Our data suggest that quasi-1D $TaSe_3$ nanowires have similar E_A values. Considering the 10× fold higher current carrying capacity and a possibility of ultimate downscaling of the quasi-1D $TaSe_3$ van der Waals material, one can consider $TaSe_3$ to be a promising material for the nanoscale interconnects.

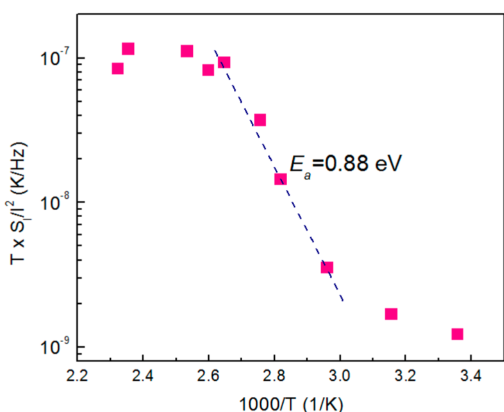

Figure 6. Temperature dependent $1/f^2$ noise analysis using the Arrhenius plot of $T \times S_I/I^2$ versus $1000/T$. The extracted electromigration activation energy for quasi-1D $TaSe_3$ nanowire is E_A = 0.88 eV.

Table 1. E_A and E_P Extracted from $1/f$ Noise Measurements for Different Technologies

technology	E_P, eV (D−H model)	E_A, eV (empirical model)
Cu direct etch	1.10[24]	
Cu with TaNTa barrier	0.76−0.78[24]	0.79[37]
Al	0.69[21]	
Al−Si (1%)	0.80[21]	
Al−Cu (4%)	0.89[21]	
Al thin film		1.14[22]
Al−Si (0.8%) passivated		0.74[39]
Al−Si (1%)−Cu (0.5%) passivated		0.78[39]
$TaSe_3$	1.0 [this work]	0.88 [this work]

One should note that the surface of the channel material can play an important role in defining the mechanism and level of $1/f$ noise. In the present study, a direct comparison between h-BN-capped and uncapped $TaSe_3$ devices was not possible. The fabricated uncapped $TaSe_3$ devices typically had non-Ohmic contacts and unstable I−V characteristics. The noise performance of such uncapped devices was affected by the current instability and non-Ohmic nature of the contacts. The effect of the surface on the noise characteristics in such a case cannot be accurately extracted, like it has been done for graphene, few-layer graphene, and MoS_2 devices.[28,29,40] However, because the thickness of $TaSe_3$ channel in the tested devices is still relatively large, and the channel material is a metal, we believe that the $1/f$ noise response is primarily defined by the "volumetric" noise.

In conclusion, we investigated the low-frequency excess noise in quasi-1D nanowires of $TaSe_3$-capped with quasi-2D h-BN layers. The $TaSe_3$ nanowires have relatively low level of the $1/f$ noise in comparison with carbon nanotubes and other low-dimensional materials. The temperature-dependent measurements revealed that the electronic excess noise becomes the $1/f^\gamma$ type with $\gamma > 1$ as temperature increases. Using the Dutta−Horn random fluctuation model of $1/f$ noise in metals and empirical model for metallic interconnects, we extracted the noise activation energy for quasi-1D $TaSe_3$ nanowires. Our results indicate that quasi-1D van der Waals materials have potential for the ultimately downscaled local interconnect applications.

Methods. *Material Preparation.* $TaSe_3$ was prepared from elemental tantalum (12.0 mmol, STREM, 99.98% purity) and selenium (35.9 mmol, STREM, 99.99% purity) with iodine (~6.45 mg/cm^3, J.T. Baker, 99.9% purity) as the transport agent. The tantalum/selenium mixture was ground and placed in a 17.78 × 1 cm fused quartz ampule (cleaned in concentrated nitric acid followed by annealing for 12 h at 900 °C). The charged reaction ampule was evacuated and backfilled with Ar 3× while submerged in an acetonitrile/dry ice bath. The flame-sealed ampule was placed in a three-zone, horizontal tube furnace heated at 20 °C min^{-1} to the final temperature gradient of 700 °C (hot zone)−680 °C (cool zone). The ampule was held at these temperatures for 2 weeks before cooling to room temperature. $TaSe_3$ crystals were removed carefully from the quartz ampule, and residual I_2 was removed by vacuum sublimation at 50 °C. The isolated yield of silver-black crystals was 90.8%. $TaSe_3$ was chemically exfoliated by sonicating 6 mg of powdered $TaSe_3$ crystals in 10 mL of ethanol for 4 h, resulting in a brownish-black suspension. This suspension was then centrifuged at 2600 rpm for 15 min, leaving well-dispersed $TaSe_3$ wires 30−80 nm wide in the supernatant.

AUTHOR INFORMATION

Corresponding Author

*E-mail balandin@ece.ucr.edu (A.A.B.).

ORCID

Guanxiong Liu: 0000-0001-8695-8671

Author Contributions

A.A.B. conceived the idea, coordinated the project, and contributed to experimental data analysis; T.T.S. supervised material synthesis and contributed to materials analysis; G.L. fabricated and tested devices, analyzed experimental data, and

DOI: 10.1021/acs.nanolett.6b04334
Nano Lett. XXXX, XXX, XXX−XXX

conducted part of the low-frequency noise measurements; M.A.B. synthesized $TaSe_3$ and conducted materials characterization; S.R. conducted noise measurements and analyzed experimental data; M.S. contributed to data analysis. All authors contributed to writing of the manuscript.

Notes

The authors declare no competing financial interest.

■ ACKNOWLEDGMENTS

This project was supported, in part, by the Emerging Frontiers of Research Initiative (EFRI) 2-DARE project: Novel Switching Phenomena in Atomic MX_2 Heterostructures for Multifunctional Applications (NSF EFRI-1433395). The nanodevice fabrication and characterization work at UC Riverside was also supported, in part, by the Semiconductor Research Corporation (SRC) and Defense Advanced Research Project Agency (DARPA) through STARnet Center for Function Accelerated nanoMaterial Engineering (FAME). The quasi-1D $TaSe_3$ devices were fabricated in the UCR Center for Nanoscale Science and Engineering (CNSE). The authors acknowledge useful discussions on $1/f$ noise with Dr. Michael Levinshtein (Ioffe Institute, St. Petersburg, Russia). S.R. acknowledges partial support from the Russian Fund for Basic Research (RFBR).

■ REFERENCES

(1) Novoselov, K. S.; Mishchenko, A.; Carvalho, A.; Castro Neto, A. H. 2D Materials and van der Waals Heterostructures. *Science* **2016**, *353*, aac9439.

(2) Geim, A. K.; Grigorieva, I. V. Van der Waals Heterostructures. *Nature* **2013**, *499*, 419−425.

(3) Novoselov, K. S.; Geim, A. K.; Morozov, S. V.; Jiang, D.; Zhang, Y.; Dubonos, S. V.; Grigorieva, I. V.; Firsov, A. A. Electric Field Effect in Atomically Thin Carbon Films. *Science* **2004**, *306*, 666−669.

(4) Zhang, Y. B.; Tan, Y. W.; Stormer, H. L.; Kim, P. Experimental Observation of The Quantum Hall Effect and Berry's Phase In Graphene. *Nature* **2005**, *438*, 201−204.

(5) Balandin, A. A. Thermal properties of graphene and nanostructured carbon materials. *Nat. Mater.* **2011**, *10*, 569−581.

(6) Li, L.; Yu, Y.; Ye, G. J.; Ge, Q.; Ou, X.; Wu, H.; Zhang, Y. Black Phosphorus Field-Effect Transistors. *Nat. Nanotechnol.* **2014**, *9*, 372−377.

(7) Teweldebrhan, D.; Goyal, V.; Balandin, A. A. Exfoliation and characterization of bismuth telluride atomic quintuples and quasi-two-dimensional crystals. *Nano Lett.* **2010**, *10*, 1209.

(8) Radisavljevic, B.; Radenovic, A.; Brivio, J.; Giacometti, V.; Kis, A. Single-layer MoS2 Transistors. *Nat. Nanotechnol.* **2011**, *6*, 147−150.

(9) Cui, X.; Lee, G. H.; Kim, Y. D.; Arefe, G.; Huang, P. Y.; Lee, C. H.; Chenet, D. A.; Zhang, X.; Wang, L.; Ye, F.; Pizzocchero, F.; Jessen, B. S.; Watanabe, K.; Taniguchi, T.; Muller, D. A.; Low, T.; Kim, P.; Hone, J. Multi-Terminal Transport Measurements of MoS_2 Using A van der Waals Heterostructure Device Platform. *Nat. Nanotechnol.* **2015**, *10* (6), 534−540.

(10) Butler, S. Z.; Hollen, S. M.; Cao, L.; Cui, Y.; Gupta, J. A.; Gutiérrez, H. R.; Heinz, T. F.; Hong, S. S.; Huang, J.; Ismach, A. F.; et al. Progress, Challenges, and Opportunities in Two-Dimensional Materials Beyond Graphene. *ACS Nano* **2013**, *7*, 2898−2926.

(11) Liu, G.; Debnath, B.; Pope, T. R.; Lake, R. K.; Salguero, T. T.; Balandin, A. A. *Nat. Nanotechnol.* **2016**, *11*, 845.

(12) Wang, Q. H.; Kalantar-Zadeh, K.; Kis, A.; Coleman, J. N.; Strano, M. S. Electronics and Optoelectronics of Two-Dimensional Transition Metal Dichalcogenides. *Nat. Nanotechnol.* **2012**, *7*, 699−712.

(13) Jariwala, D.; Sangwan, V. K.; Lauhon, L. J.; Marks, T. J.; Hersam, M. C. Emerging Device Applications for Semiconducting Two-Dimensional Transition Metal Dichalcogenides. *ACS Nano* **2014**, *8*, 1102−1120.

(14) Ferrari, A. C.; Bonaccorso, F.; Falko, V.; Novoselov, K. S.; Roche, S.; Bøggild, P.; Borini, S.; Koppens, F.; Palermo, V.; Pugno, N.; et al. Science and Technology Roadmap for Graphene, Related Two-Dimensional Materials and Hybrid Systems. *Nanoscale* **2015**, *7*, 4598−4810.

(15) Lipatov, A.; Wilson, P. M.; Shekhirev, M.; Teeter, J. D.; Netusil, R.; Sinitskii, A. Few-layered titanium trisulfide (TiS3) field-effect transistors. *Nanoscale* **2015**, *7* (29), 12291−12296.

(16) Island, J. O.; Buscema, M.; Barawi, M.; Clamagirand, J. M.; Ares, J. R.; Sanchez, C.; Ferrer, I. J.; Steele, G. A.; van der Zant, H. S. J.; Castellanos-Gomez, A. Ultrahigh Photoresponse of Few-Layer TiS3 Nanoribbon Transistors. *Adv. Opt. Mater.* **2014**, *2*, 641−645.

(17) Island, J. O.; Barawi, M.; Biele, R.; Almazan, A.; Clamagirand, J. M.; Ares, J. R.; Sanchez, C.; van der Zant, H. S. J.; Alvarez, J. V.; D'Agosta, R.; Ferrer, I. J.; Castellanos-Gomez, A. TiS3 Transistors with Tailored Morphology and Electrical Properties. *Adv. Mater.* **2015**, *27* (16), 2595−2601.

(18) Stolyarov, M. A.; Liu, G.; Bloodgood, M. A.; Aytan, E.; Jiang, C.; Samnakay, R.; Salguero, T. T.; Nika, D. L.; Rumyantsev, S. L.; Shur, M. S.; Bozhilov, K. N.; Balandin, A. A. Breakdown Current Density in h-BN-Capped Quasi-1D $TaSe_3$ Metallic Nanowires: Prospects of Interconnect Applications. *Nanoscale* **2016**, *8*, 15774−15782.

(19) Balandin, A. A. *Nat. Nanotechnol.* **2013**, *8*, 549−555.

(20) von Haartman, M.; Ostling, M. *Low-Frequency Noise in Advanced MOS Device*; Springer: Dordrecht, The Netherlands, 2007.

(21) Koch, R. H.; Lloyd, J. R.; Cronin, J. 1/f Noise and Grain-Boundary Diffusion in Aluminum and Aluminum Alloys. *Phys. Rev. Lett.* **1985**, *55*, 2487−2490.

(22) Chen, T.-M.; Yassine, A. M. Electrical Noise and VLSI Interconnect Reliability. *IEEE Trans. Electron Devices* **1994**, *41*, 2165−2172.

(23) Neri, B.; Diligenti, A.; Bagnoli, P. E. Electromigration and Low-Frequency Resistance Fluctuations in Aluminum Thin-Film Interconnections. *IEEE Trans. Electron Devices* **1987**, *34*, 2317−2322.

(24) Beyne, S.; Croes, K.; De Wolf, I.; Tőkei, Zs. 1/f Noise Measurements for Faster Evaluation of Electromigration in Advanced Microelectronics Interconnections. *J. Appl. Phys.* **2016**, *119*, 184302.

(25) Vandamme, L. K. J. Noise as a Diagnostic Tool for Quality and Reliabiltiy of Electroic Devices. *IEEE Trans. Electron Devices* **1994**, *41*, 2176−2187.

(26) Neri, B.; Ciofi, C.; Dattilo, V. Noise and Fluctuations in Submicrometric Al-Si Interconnect lines. *IEEE Trans. Electron Devices* **1997**, *44*, 1454−1459.

(27) Guo, J.; Jones, B. K.; Trefan, G. The Excess Noise in Integrated Circuit Interconnects Before and after Electromigration Damage. *Microelectron. Reliab.* **1999**, *39*, 1677−1690.

(28) Liu, G.; Rumyantsev, S.; Shur, M. S.; Balandin, A. A. Origin of 1/f Noise in Graphene Multilayers: Surface vs. Volume. *Appl. Phys. Lett.* **2013**, *102*, 093111. Rumyantsev, S.; Liu, G.; Stillman, W.; Shur, M.; Balandin, A. A. Electrical and Noise Characteristics of Graphene Field-Effect Transistors: Ambient Effects, Noise Sources and Physical Mechanisms. *J. Phys.: Condens. Matter* **2010**, *22*, 395302−395307.

(29) Rumyantsev, S. L.; Jiang, C.; Samnakay, R.; Shur, M. S.; Balandin, A. A. 1/f Noise characteristics of MoS2 thin-film transistors: Comparison of single and multilayer structures. *IEEE Electron Device Lett.* **2015**, *36*, 517.

(30) Snow, E. S.; Novak, J. P.; Lay, M. D.; Perkins, F. K. 1/f Noise in Single-Walled Carbon Nanotube Devices. *Appl. Phys. Lett.* **2004**, *85*, 4172−4174.

(31) Rumyantsev, S.; Vijayaraghavan, A.; Kar, S.; Khanna, A.; Soldano, C.; Pala, N.; Vajtai, R.; Nalamasu, O.; Shur, M.; Ajayan, P. 14th International Symposium, "Nanostructures: physics and technology", St. Petersburg, June 26−30, 2006.

(32) Vijayaraghavan, A.; Kar, S.; Rumyantsev, S.; Khanna, A.; Soldano, C.; Pala, N.; Vajtai, R.; Kanzaki, K.; Kobayashi, Y.; Nalamasu, O.; Shur, M.; Ajayan, P. *J. Appl. Phys.* **2006**, *100*, 024315.

DOI: 10.1021/acs.nanolett.6b04334
Nano Lett. XXXX, XXX, XXX−XXX

(33) Shur, M.; Rumyantsev, S.; Liu, G.; Balandin, A. A. Electrical and Noise Characteristics of Graphene Field-Effect, (invited), ICNF 2011, Toronto, Canada, June 12−16 2011, Proc.: IEEE Xplore 145−149.

(34) Xu, Y.; Huang, L.; Chen, G.; Wu, F.; Xia, W.; Liu, H. Electromigration — Induced Failure Mechanism and Lifetime Prediction in NiCu Thin Film. *Electronic Packaging Technology (ICEPT) 2014 15th International Conference on* **2014**, 1071−1074.

(35) Dutta, P.; Horn, P. Low-Frequency Fluctuation in Solids: 1/f Noise. *Rev. Mod. Phys.* **1981**, *53*, 497−516.

(36) Dutta, P.; Dimon, P.; Horn, P. M. Energy Scales for Noise Processes in Metals. *Phys. Rev. Lett.* **1979**, *43*, 646−649.

(37) Tang, B. J.; Croes, K.; Simoen, E.; Beyne, S.; Adelmann, C.; Tőkei, Zs. Experimental Validation of Electromigration by Low Frequency Noise Measurement for Advanced Copper Interconnects Application. *Noise and Fluctuations (ICNF), 2015 International Conference on* **2015**, 1−4.

(38) Cottle, J. G.; Chen, T. M.; Rodbell, K. P. A Comparison between Noise Measurements and Conventional Electromigration Reliability Testing, Pioc 26th Re1 Phys. Symp. 1988; pp 203−208.

(39) Bagnoli, P. E.; Ciofi, C.; Neri, B.; Pennelli, G. Electromigration in Al Based Stripes: Low Frequency Noise Measurements and MTF Tests. *Microelectron. Reliab.* **1996**, *36*, 1045−1050.

(40) Stolyarov, M. A.; Liu, G.; Rumyantsev, S. L.; Shur, M.; Balandin, A. A. Suppression of 1/f noise in near-ballistic h-BN-graphene-h-BN heterostructure field effect transistors. *Appl. Phys. Lett.* **2015**, *107*, 023106.

DOI: 10.1021/acs.nanolett.6b04334
Nano Lett. XXXX, XXX, XXX−XXX